LANGMUIR

pubs.acs.org/Langmuir Article

Load Impedance of Immersed Layers on the Quartz Crystal Microbalance: A Comparison with Colloidal Suspensions of Spheres

Marc Meléndez,* Adolfo Vázquez-Quesada, and Rafael Delgado-Buscalioni*

Cite This: https://dx.doi.org/10.1021/acs.langmuir.0c01429 Read Online

ACCESS | Metrics & More | Article Recommendations

ABSTRACT: The analytical theories derived here for the acoustic load impedance measured by a quartz crystal microbalance (QCM), due to the presence of layers of different types (rigid, elastic, and viscous) immersed in a fluid, display generic properties, such as "vanishing mass" and positive frequency shifts, which have been observed in QCM experiments with soft-matter systems. These phenomena seem to contradict the well-known Sauerbrey relation at the heart of many QCM measurements, but here, we show that they arise as a natural consequence of hydrodynamics. We compare our one-dimensional immersed plate theory with three-dimensional simulations of rigid and flexible submicron-sized suspended spheres and with experimental results for adsorbed micron-sized colloids, which yield a "negative acoustic mass". The parallel behavior unveiled indicates that the QCM response is highly sensitive to hydrodynamics, even for adsorbed colloids. Our conclusions call for a revision of existing theories based on adhesion forces and elastic stiffness at contact, which should, in most cases, include hydrodynamics.

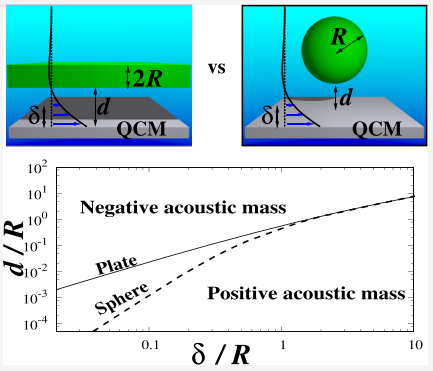

INTRODUCTION

Quartz crystal microbalances (QCM) principally consist of a thin quartz crystal between two electrodes. Being a piezoelectric material, the quartz oscillates in response to an AC current. In many devices, the crystal is cut in such a way that transverse vibrations take place parallel to the free surface. Because of the oscillatory motion, we would reasonably expect (correctly, as it turns out) that increasing the mass slightly by adding a small layer onto the surface of the QCM will lead to a small decrease in the frequency of oscillation, f. For a harmonic oscillator of mass M, we can easily prove to ourselves that a small increase in the mass ΔM causes a decrease in the frequency

$$\frac{\Delta f}{f} = -\frac{1}{2}\frac{\Delta M}{M} \tag{1}$$

In 1959, Sauerbrey derived a similar equation for the QCM.[1] With Δm representing mass per unit area deposited on the QCM

$$\frac{\Delta f}{f} = -\frac{2f_0 \Delta m}{Z_Q} \tag{2}$$

Typically, for AT-cut crystals, the fundamental frequency equals $f_0 = 5$ MHz, the acoustic impedance of the quartz $Z_Q = 8.8 \times 10^6$ kg/(m^{2}s), and f represents the working frequency. As frequency shifts may be measured with great accuracy, much experimental work has relied on the QCM as an extremely sensitive mass detector, hence its name.

QCMs also work in contact with fluids, as demonstrated by Nomura and Okuhara,[2] who showed that the transverse waves propagate into a fluid (of density ρ and shear viscosity η) with a heavy damping. Thus, QCMs with dissipation monitoring (QCM-D) instruments measure both the frequency of oscillation and the energy dissipation in a ring-down experiment, in which the AC voltage is turned off and the quartz crystal allowed to come to rest. Because the damping occurs within tens of microseconds, a series of consecutive ring-downs can monitor the evolution of molecular processes taking place over second or minute timescales. As a consequence, QCM-D instruments have become a standard tool for biosensing systems of supported membranes and Langmuir−Blodgett and protein and liposome films, among others.[3−6] In this context, Gizeli's group observed that, for some systems, the ratio of the dissipation to the frequency shift, which they termed the acoustic ratio, did not depend on the concentration of molecules deposited on the QCM, suggesting that it was a property of the geometry of the molecules, rather than the mass of the deposited film.[3]

When thinking in terms of the Sauerbrey relation, one would never conceive of an increase in the load leading to an increased

Received: May 19, 2020
Revised: July 9, 2020
Published: July 14, 2020

frequency of vibration, but this has in fact been observed in experiments with massive (micron-sized) particles.[7−10] A widely repeated explanation for these "negative Sauerbrey masses" states that an increase in the frequency shift (*i.e.*, a "negative acoustic mass") arises as a consequence of a very fast response of the analyte-wall contact, modeled by an (generally complex) effective spring.[3] However, this explanation does not take into account the hydrodynamic transport of momentum.

Historically, hydrodynamic effects have often been disregarded in QCM research, even though some works have proven that they affect the outcome of QCM measurements. Pioneering simulation studies in two-dimensional setups were able to reproduce the previously unexplained response of QCM experiments with discrete particles with sizes of the order of tens of nanometers, such as the decrease of the acoustic ratio with the frequency shift.[11] Researchers have started to recognize the relevance of hydrodynamics in the QCM,[12] and recent three-dimensional simulations have examined, for instance, the nonmonotonous relation between the dissipation and the coverage,[13] the effect of adsorbed particle shapes,[14] or the strong sensitivity to the mass distribution over the resonator.[15] Notably, when discrete particles become highly packed forming a film (dense limit), hydrodynamic simulations indicate that the Sauerbrey limit is recovered (zero dissipation), and this leads to a method to estimate particle size.[16] As we shall see below, the acoustic ratio may well diverge or change sign naturally, even for moderately small loads suspended in a fluid.

Although previous research has developed one-dimensional phenomenological models of the viscoelasticity of films,[6] recent experiments with nanoparticles, liposomes, viruses, and DNA strands have shown strong deviations from these theories.[3,18−21]

Following most of the previous work in the field, we make use of the small load approximation,[4] which allows us to write the complex frequency shift in terms of the load impedance.

$$\Delta f + \mathrm{i}\Delta\Gamma = \frac{\mathrm{i}f_0}{\pi}\frac{Z_\mathrm{L}}{Z_\mathrm{Q}} \tag{3}$$

Here, $\Delta\Gamma$ is the change in the decay rate of the resonator, and the complex load impedance Z_L equals the stress phasor on the QCM surface divided by its velocity phasor.

The main point in the present article is that the primary effect determining the impedance of suspensions measured by the QCM involves the change in the hydrodynamic motion of the fluid due to the presence of suspended matter. To argue for this statement, we derived an analytical theory for the effect of an infinite immersed layer on the motion of a QCM, represented by a flat horizontal oscillating plane at $z = 0$ in contact with a fluid filling the space $z > 0$. We also show that the changes in impedance as a function of distance and frequency for a suspended membrane resemble the changes observed for a sparse periodic array of spheres. The data for spheres were produced by our QCM simulations of suspended liposomes using the FLUAM code,[22] which is based on Peskin's immersed boundary method.[23] We have shown elsewhere that our simulations agree with experimental results.[15,17] In addition, we have considered the crossover to a positive frequency shift ("negative acoustic mass"). Comparing the analytical prediction of the plate system with our simulations of submicron spheres and experiments carried out with micron-sized colloids leads to several interesting conclusions discussed below.

MATERIALS AND METHODS

Our mesoscopic simulation algorithm, implemented for the GPU code FLUAM ("FLUid And Matter interaction"),[22,38] solves the Navier−Stokes equations with a second-order-accurate finite-volume scheme on a staggered grid. The fluid−matter interaction is achieved using Peskin's immersed boundary method.[23]

The simulated suspended spheres were constructed with small bead-like volume elements connected by means of an elastic network that linked neighboring beads with harmonic springs. Each simulation placed the sphere with the desired separation from the QCM surface, d, into an $L \times L \times L_z$ simulation box with periodic boundary conditions in the x and y directions. L was chosen significantly larger than δ to avoid hydrodynamic interactions among the sphere and its periodic images. L_z was chosen larger than 3δ to minimize the effect of the upper limit of the box, where the fluid velocity was set to zero. Below the sphere, the QCM surface performed several oscillations until the fluid reached a periodic oscillation pattern. The suspended sphere remained free to move in response to the fluid traction. The stress at the interface was then calculated by taking the numerical derivative of the fluid velocity with height z on the QCM surface. For more details on the simulation methods, please refer to our work on the hydrodynamics of tethered liposomes.[15] The results presented here were computed on our own group's GPU cluster.

All experimental data points were taken from experiments reported previously in the literature and are referenced below.

RESULTS AND DISCUSSION

Oscillating Boundary Layer. We wish to study fluid systems near a vibrating plane wall in the Stokes flow regime.[24] Our fluid, with density ρ and shear viscosity η, obeys the equations of linear hydrodynamics and lies in the space above the $z = 0$ plane. Furthermore, the translational symmetry of the problem ensures that the flow velocity $\tilde{u}(z, t)$ will depend only on the z coordinate and time. The equation describing the velocity field reads[24−26]

$$\frac{\partial\tilde{u}}{\partial t} = \frac{\eta}{\rho}\frac{\partial^2\tilde{u}}{\partial z^2} \tag{4}$$

We will mark time-dependent oscillating functions with tildes and rely on phasors to represent the amplitudes of the steady-state solutions

$$\tilde{u}(z, t) = \mathrm{Re}(u(z)e^{-\mathrm{i}\omega t}) \tag{5}$$

with the complex-valued phasor amplitude $u(z)$[25]

$$u(z) = Ae^{-\alpha z} + Be^{\alpha z} \tag{6}$$

where $\alpha = (1 - i)/\delta$, and $\delta = \sqrt{2\eta/(\omega\rho)}$ measures the depth of penetration of the oscillating flow. Assume the wall vibrates with frequency ω. If we apply stick boundary conditions where the fluid meets the plane and add that the velocity vanishes far from it, then

$$u(0) = u_0 \tag{7}$$

$$\lim_{z\to\infty} u(z) = 0 \tag{8}$$

The coefficient u_0 may take, in general, complex values. By applying the boundary conditions to the general solution, we see that $A = u_0$ and $B = 0$, which implies a velocity phasor

$$u_\mathrm{f}(z) = u_0e^{-\alpha z} \tag{9}$$

for the Stokes flow.

We now calculate the impedance associated with the Stokes flow, Z_f. According to the standard definition, Z_f is the ratio of

https://dx.doi.org/10.1021/acs.langmuir.0c01429
Langmuir XXXX, XXX, XXX−XXX

the shear stress exerted on the plane to its velocity. Let $\sigma = \eta \frac{\partial u}{\partial z}\Big|_{z=0}$ represent the phasor amplitude of the stress.

$$Z_f = \frac{\sigma}{u(0)} = \frac{\eta \frac{\partial u}{\partial z}\Big|_{z=0}}{u_0} = -\eta\alpha \tag{10}$$

The subscript f distinguishes the impedance of the base Stokes flow from other load impedances calculated below.

Immersed Rigid Plate. Now imagine a solid horizontal plate of thickness a and mass density ρ' placed above the vibrating plane at a distance d (Figure 1a). The fluid will transmit

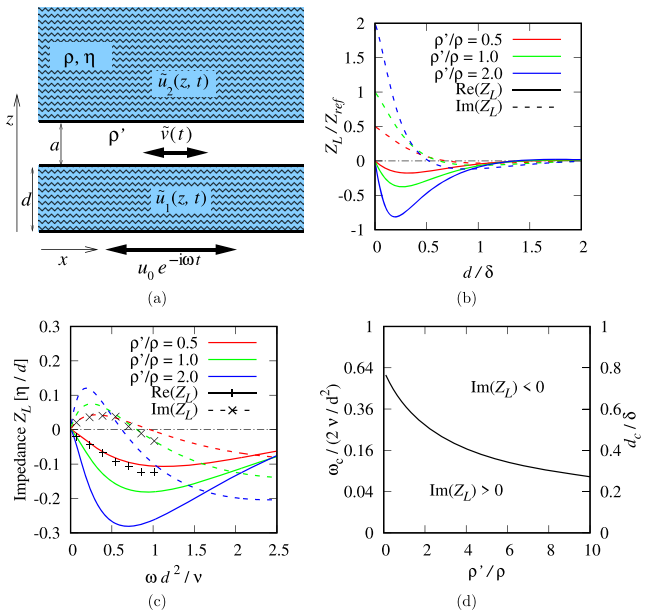

Figure 1. (a) Schematic representation of a rigid horizontal plate of density ρ' and thickness a immersed in a fluid of density ρ and shear viscosity η above an oscillating plane. (b) Complex impedance Z_L due to the presence of the plate in (a) *vs* distance d between the plate and plane in units of $\delta = \sqrt{2\nu/\omega}$ (the kinematic viscosity equals $\nu = \eta/\rho$). The curves correspond to the real (solid) and imaginary (dashed) parts of the impedance (divided by the Sauerbrey value $Z_{ref} = \omega\rho' a$). (c) Load impedance *vs* dimensionless parameter $\omega d^2/\nu$ for three different plate densities. The solid line plots $\mathrm{Re}(Z_L)$, while the dashed line corresponds to $\mathrm{Im}(Z_L)$. The thickness was chosen equal such that $d/a = 1$. The experimental points for silica particles with a radius of half a micron in a 150 mM KCl electrolyte were taken from the study by Olsson *et al.*[27] (setting d = 50 nm for a qualitative comparison). (d) Frequency ω_c and height d_c at which the imaginary part of the impedance crosses the horizontal axis [see (b)] *vs* the ratio of the plate density to the fluid density. Please note that the scale on the left is not linear. Equation 20 implies that changing ρ'/ρ is equivalent to changing a while leaving ρ'/ρ fixed.

the motion of the vibrating lower plane and drag the suspended layer along. Having reached a stationary oscillation, the plate will move with velocity

$$\tilde{v}(t) = v_0 e^{-i\omega t} \tag{11}$$

with a complex factor v_0 to be determined below. The motion of the solid layer results from the shear stress exerted by the fluid from above and below. Let $\tilde{u}_i(z,t)$ represent the velocity fields in the regions below $(i = 1)$ and above $(i = 2)$ the plate. Then we can rewrite Newton's equation of motion

$$\rho' a \frac{d\tilde{v}}{dt} = \eta\left(\frac{\partial \tilde{u}_2}{\partial z}\Big|_{z=d+a} - \frac{\partial \tilde{u}_1}{\partial z}\Big|_{z=d}\right) \tag{12}$$

in terms of phasor amplitudes

$$-i\omega\rho' a v_0 = \eta\left(\frac{\partial u_2}{\partial z}\Big|_{z=d+a} - \frac{\partial u_1}{\partial z}\Big|_{z=d}\right) \tag{13}$$

Clearly, the fluid above the plate obeys the equations of Stokes flow already calculated above, but this time with an amplitude given by the motion of the plate.

$$u_2(z) = v_0 e^{-\alpha(z-(d+a))} \tag{14}$$

For the lower wall, we substitute the form of the general solution 6 into boundary conditions, which ensure that the fluid moves at the same speed as the walls at the point of contact.

$$u_1(0) = u_0 = A + B \tag{15}$$

$$u_1(d) = v_0 = Ae^{-\alpha d} + Be^{\alpha d} \tag{16}$$

The extra load impedance due to the plate, Z_L, equals the total impedance minus the impedance due to the base Stokes flow Z_f

$$Z_L = \frac{\sigma}{u_0} - Z_f = 2\alpha\eta\frac{B}{u_0} \tag{17}$$

From the boundary conditions 15 and 16, we obtain A and B as a function of the plate and resonator velocity amplitudes, v_0 and u_0, and write the load impedance as

$$Z_L = \frac{\alpha\eta}{\sinh(\alpha d)}\frac{1}{u_0}(v_0 - u_f(d)) \tag{18}$$

Thus, a solid plate creates an impedance proportional to the difference between the plate velocity v_0 and the (unperturbed) Stokes flow velocity 9 at the lower fluid−plate interface $(z = d)$. Equation 18 leads to the conclusion that a fixed plate $(v_0 = 0)$ yields an impedance inversely proportional to $1 - e^{2\alpha d}$ and that the load impedance vanishes if the plate moves with the base Stokes flow $(v_0 = u_f(d))$. In the limiting case of a small gap between the vibrating wall and plate, $\alpha d \ll 1$, the load impedance corresponds to that of a Couette flow created by the perturbative velocity $v_0 - u_f(d)$ in a gap of width d

$$Z_L = \eta\left(\frac{v_0 - u_f(d)}{d}\right), \qquad \text{for } d \ll \delta \tag{19}$$

All that remains now is to determine v_0 as a function of u_0. To this end, we substitute the general solution for Stokes flow 6 into the equation of motion for the wall 13 and use the result in combination with the boundary conditions to solve for v_0. Substituting the result into eq 18

$$Z_L = \frac{\omega\rho' a}{\frac{\omega\rho' a}{2\alpha\eta}(e^{-2\alpha d} - 1) - i}e^{-2\alpha d} \tag{20}$$

Note that when the distance between the plate and the lower plane vanishes, we recover a Sauerbrey-like relation, $\lim_{d\to 0} Z_L = i\omega\rho' a$, with a purely imaginary impedance, corresponding to a frequency shift proportional to the deposited mass $\rho' a$. The opposite limit obviously leads to a vanishing load impedance, $\lim_{d\to\infty} Z_L = 0$. Below, we will often use the Sauerbrey impedance, $Z_{ref} = \omega\rho' a$, as a reference to scale our results.

https://dx.doi.org/10.1021/acs.langmuir.0c01429
Langmuir XXXX, XXX, XXX−XXX

Diverging and Negative Acoustic Ratios. Figure 1b plots the load impedance as a function of the height d for three different plate densities. As already mentioned, within the small load approximation 3, the dimensionless acoustic ratio (defined as the ratio of the dissipation to the frequency shift) is proportional to $-2Re(Z_L)/\mathrm{Im}(Z_L)$. In the experimental work, it is customary to present a ratio of the dissipation ΔD to the frequency shift Δf, related to the dimensionless acoustic ratio by

$$-\frac{\Delta D}{\Delta f} = -\frac{2}{f_n}\frac{\mathrm{Re}(Z_L)}{\mathrm{Im}(Z_L)} \tag{21}$$

where f_n is the frequency of the harmonic used in experiments. Therefore, if the imaginary part of Z_L changes sign as a consequence of the variation of some parameter, the acoustic ratio will diverge and become negative after the divergence.

Positive frequency shifts (negative Sauerbrey masses) show up in experiments when analyzing massive particles above a certain crossover frequency ω_c. The simple plate model also displays such an inversion of the sign of Z_L. In particular, Figure 1c shows that the plate qualitatively behaves like experiments with micron-sized colloids. The plate load impedance is compared there to measurements of silica particles of radius $R = 0.5\ \mu$m adsorbed to a silica surface in a K^+Cl^- electrolyte at a concentration of 150 mM.[27] The similarity between the particle and plate suggests that the load impedance results principally from hydrodynamic stress, in contrast to previous research, which had attributed the effect to contact forces between the surface and the load.[3,7,9,27] We will return to this important point below.

Rescaling the load impedance by Z_{ref} leaves us with an expression that depends only on the dimensionless parameters ρ'/ρ, a/δ, and d/δ.

$$\frac{Z_L}{Z_{ref}} = \frac{e^{-2(1-i)d/\delta}}{\frac{1+i}{2}\frac{\rho'}{\rho}\frac{a}{\delta}(e^{-2(1-i)d/\delta}-1)-i} \tag{22}$$

Because $\delta^2 \propto \omega^{-1}$, doubling the layer width a and the distance d has the same effect as multiplying the frequency ω by four. Thus, for any fixed frequency, we expect to observe a diverging acoustic ratio ($\mathrm{Im}(Z_L) = 0$) for some large enough distance d_c (Figure 1d). Similarly, large enough analytes ($a > a_c$) yield negative frequency shifts for given values of ω and d. Setting $\mathrm{Im}(Z_L) = 0$ leads to the following relation among the dimensionless parameters

$$\frac{\rho'}{\rho}\frac{a_c}{\delta_c} = \frac{2\cos\left(2\frac{d_c}{\delta_c}\right)}{e^{-2d_c/\delta_c}\left(\cos\left(2\frac{d_c}{\delta_c}\right)-\sin\left(2\frac{d_c}{\delta_c}\right)\right)} \tag{23}$$

where we have used the subindex c as a reminder that we mean crossover values. We will illustrate the generality of the hydrodynamic effect below by comparing this prediction to simulations of immersed spheres and experiments with colloidal particles.

Hydrodynamic Origin of "Negative Acoustic Masses". To understand why the hydrodynamic perturbation of the analyte may produce a positive frequency shift (or equivalently a "negative acoustic mass"), let us consider the tangential hydrodynamic stress on the surface. Without loss of generality, suppose the resonator is moving with a velocity $u_0\cos(\omega t)$, with u_0, a real number. The observed stress $\tilde{\sigma}(t)$ can be decomposed into in-phase and out-of-phase components, proportional to the real and imaginary parts of the stress phasor, $\tilde{\sigma}(t) = Re(\sigma e^{-i\omega t})$. Now, for phase angles $\theta = \omega t$ equal to integer multiples of 2π, the resonator velocity reaches its maximum value, $|u_0|$, as its displacement crosses the midpoint of the oscillation. At this precise moment, the observed stress equals $\tilde{\sigma}(2\pi n/\omega) = Re(\sigma)$, revealing the dissipative part of the stress. A quarter of a cycle later, $(\theta = 2\pi n + \pi/2)$, the observed stress equals $\tilde{\sigma}((2\pi n + \pi/2)/\omega) = \mathrm{Im}(\sigma)$, which unveils the fate of the frequency shift. If $\mathrm{Im}(\sigma) > 0$, the extra stress created by the analyte tends to pull the resonator forward (along $x > 0$), thus decreasing its frequency (positive acoustic mass). The opposite change takes place when $\mathrm{Im}(\sigma) < 0$. In other words, the "acoustic mass" or the frequency shift simply emerges from the phase lag between the resonator velocity and the extra stress coming from the analyte. This phase lag is proportional to the time required by viscous diffusion to propagate the surface stress from the plate at $z = d$ to the wall at $z = 0$.

To visualize the impedance in terms of the flow, consider the velocity profiles drawn in Figure 2. The red dashed-dotted lines

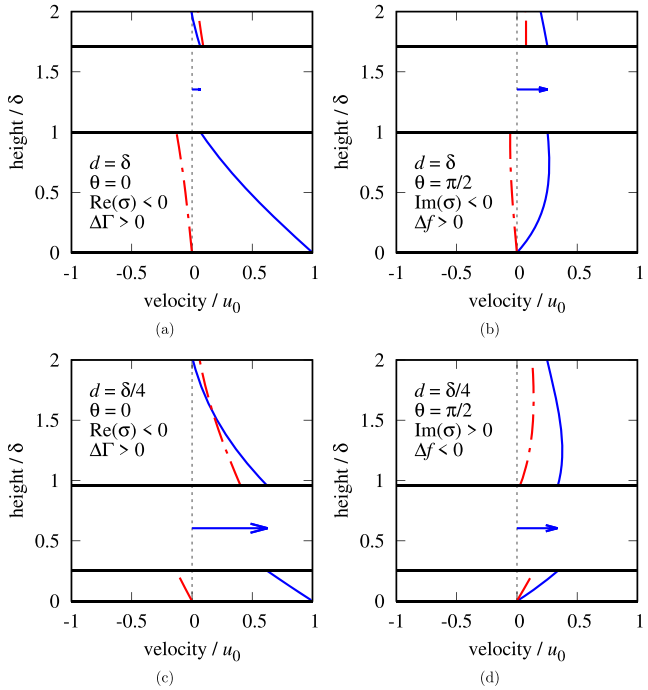

Figure 2. Velocity profiles for two different distances between the plate and the oscillating lower plane [top row (a,b): $d = \delta$, bottom row (c,b): $d = \delta/4$]. The left column (a,c) shows the velocities at a $\theta = \omega t = 0$ rad phase angle, and the right column (b,d) corresponds to a phase angle of $\theta = \omega t = \pi/2$ rad. The arrows indicate the velocity of the plate. The solid blue line plots the velocity of the fluid at different heights, and the dashed-dotted red line indicates the perturbation of the Stokes flow u_p from eq 24 due to the presence of the immersed plate.

correspond to the perturbation $\tilde{u}_p(z, t)$ of the laminar Stokes flow 6 due to the presence of the immersed plate.

$$\tilde{u}_p(z, t) = \tilde{u}_j(z, t) - (u_0 e^{-\alpha z})e^{-i\omega t} \tag{24}$$

where j equals 1 or 2 depending on whether we focus on the fluid below the plate ($z < d$) or above it ($z > d + a$). Because the extra hydrodynamic stress caused by the plate is $\tilde{\sigma} = \eta\partial_z\tilde{u}_p$, the real part of Z_L is proportional to the derivative of $\tilde{u}_p$ with z at a phase angle of $\theta = \omega t = 0$ rad, while the imaginary part corresponds to the derivative at phase angle $\theta = \pi/2$ rad. In the figure, the sign of Z_L

https://dx.doi.org/10.1021/acs.langmuir.0c01429
Langmuir XXXX, XXX, XXX−XXX

and the surface stress $\tilde{\sigma}$ depends on the slope of the red dashed-dotted line representing $\tilde{u}_p$ with respect to the vertical dotted line, which stands for no perturbation ($\tilde{\sigma} = 0$). Notice that at $\theta = \pi/2$, the slope at $z = 0$ in the top right figure has a sign opposite to that of the bottom right one, indicating the change in the imaginary part of Z_L. The top panel corresponds to a positive frequency shift Δf, while the bottom panel yields $\Delta f < 0$. In other words, the top row leads to a "negative acoustic mass", while the bottom row produces a positive result.

Comparing Immersed Plates with Suspended Spheres. *Impedances.* Comparing the impedance curve for a solid plate to simulation data for three-dimensional suspended spheres leads to some interesting and surprising observations. As mentioned in the Materials and Methods section, these simulations were performed using the immersed boundary method[22,23] with periodic boundary conditions in the x and y directions (resonator plane) and introducing no-slip rigid planes at the top and bottom of the simulation box. The oscillating flow was imposed at the bottom of the box, and the velocity was set to zero at the top. The analytical expression for the contribution of the upper boundary to the impedance results from eq 18, setting $v_0 = 0$ and d equal to the box height. Both theory and simulations confirm that the change in the impedance due to a stationary upper wall remains negligible when the box height exceeds about 3δ.

Figure 3a,b illustrates the proportionality between the impedance due to a small sphere ($R = 0.16\delta$ in the figures) and that of a rigid plate at the same height as the center of the sphere. The parallel behaviors remain similar up to distances surprisingly close to the wall.

A large sphere qualitatively changes the behavior of the impedance near the wall. While an immersed plate feels the effect of the flow only at height d (remember that the thickness of the plate plays no role as long as we fix the value of $\rho' a$), the drag on the sphere comes from the different flow velocities in the range $z \in [d - R, d + R]$, which we can only neglect when $R \ll \delta$. A simple way to approximate the response of a sphere with this one-dimensional model, though, consists in forcing the immersed plate to move in such a way that its lateral displacement mirrors that of a sphere of radius R at height d in response to the oscillating flow.

In the steady state, the sphere vibrates with frequency ω

$$x(t) = x_0 e^{-i\omega t} \tag{25}$$

To determine x_0, we substitute $x(t)$ into Newton's second law

$$-m\omega^2 x_0 = i\omega\zeta x_0 + 6\pi\eta r\left[(1 + \alpha r)\overline{v}_s + \frac{1}{3}\alpha^2 r^2 \overline{v}_v\right] \tag{26}$$

The force phasor amplitude on the right was calculated by Mazur and Bedeaux.[28] The friction ζ stands for

$$\zeta = 6\pi\eta r\left(1 + \alpha r + \frac{1}{9}\alpha^2 r^2\right) \tag{27}$$

and $\overline{v}_s$ and $\overline{v}_v$ for averages of the unperturbed flow over the surface and volume of the sphere, respectively. Their analytical expressions are derived in Appendix A. Solving eq 26 for the phasor describing the motion of the sphere, we get

$$x_0 = \frac{6\pi\eta r\left[(1 + \alpha r)\overline{v}_s + \frac{1}{3}\alpha^2 r^2 \overline{v}_v\right]}{-m\omega^2 - i\omega\zeta} \tag{28}$$

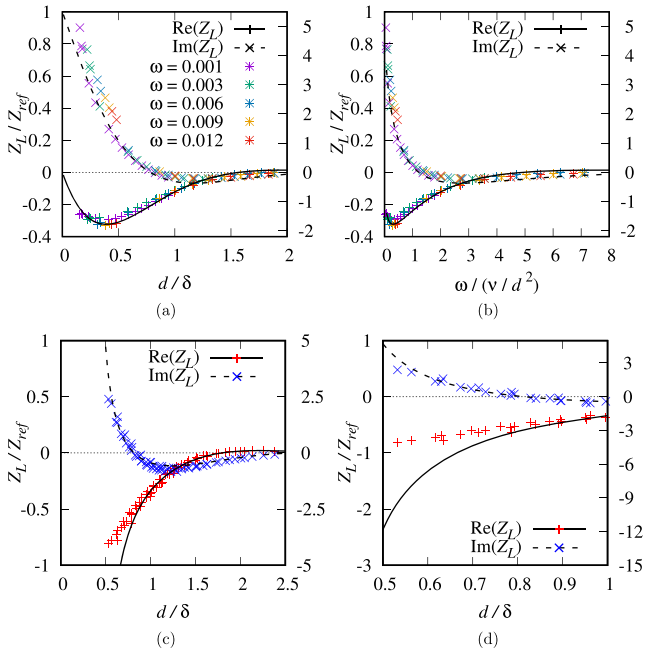

Figure 3. (a) Load impedance obtained from numerical simulations of a suspended neutrally buoyant sphere of radius $R = 0.16\delta$ in a $(L \times L \times L_z) = (1.33 \times 1.33 \times 5.34)\delta^3$ box with periodic boundaries in the x and y directions *vs* the height of its center (points, impedance scale on the right axis) compared to the impedance of a plate (curves, left axis) *vs* its distance to the oscillating plane. Results are scaled with the Sauerbrey impedance, $Z_{ref} = m\omega$, where the masses per unit surface $m = (4\pi/3)R^3\rho'/L^2$ (sphere) and $m = \rho' a$ (plate) were chosen equal to each other. The data were obtained from simulations at different frequencies. (b) Load impedance *vs* frequency for the small sphere in (a). Points represent simulation data (right axis), and curves represent the analytical result for the solid plate (left axis). (c) Impedance of a sphere with radius $R = 0.526\delta$ (points corresponding to the right axis) as a function of the distance d between its center and the wall. The curves correspond to the left axis and show the impedance caused by a plane at height d with the same lateral motion as that of a sphere. (d) Close up of (c) for simulations with the sphere close to the wall.

The velocity phase amplitude equals $v_0 = -i\omega x_0$; so, the corresponding load impedance follows from eq 18 writing v_0 in terms of the x_0 given above. Plotting the impedance for a sphere with a diameter comparable to the penetration depth, $R/\delta = 0.526$, produces the curves in Figure 3c. Once again, apart from the vertical scaling factor, the curves agree as the sphere moves away from the wall, even though we are comparing its impedance to that of a plane.

Equation 26 works well far from the wall but breaks down close to it. As Mazur and Bedeaux themselves pointed out,[28] the theory does not take into account the hydrodynamic reflections that significantly modify the Stokes flow felt by the sphere when it approaches the resonator surface. Figure 3d confirms that the approximate theory and simulations significantly disagree near the oscillating wall.

Concerning the opposite case, when particles float far enough from the wall, the impedance corresponds to a positive frequency shift (see Figure 3a), which might be revealed in kinetic experiments as a transient increase in Δf once the colloidal particles start to populate the $\mathrm{Im}(Z_L) < 0$ region. This scenario, more likely to occur for larger particles ($R \sim 100$ nm), is however challenging to observe in experiments[a] because, rather than a single-particle impedance, QCM senses ensemble-averaged quantities. In practice, the measured impedance

https://dx.doi.org/10.1021/acs.langmuir.0c01429
Langmuir XXXX, XXX, XXX−XXX

emerges from the combined impedances of all the suspended particles. For instance, consider particles of $R < 200$ nm: those located very close to the surface $z < z_c$ or adsorbed to it will contribute with a large positive impedance $\mathrm{Im}(Z_L) > 0$, which might overpower the net contribution of particles above z_c. Moreover, for suspensions with higher concentrations, colloid−colloid hydrodynamic interactions will somewhat modify the impedance in ways which are still being actively investigated.[11,13,20]

Zero-Frequency Shift. The crossing over to positive frequency shifts ($\mathrm{Im}(Z_L) < 0$) has received attention in experimental research, where it has been viewed as a proxy for interactions between large particles and the substrate.[3,7,9,27] Figure 4 presents the scaled crossover separation between

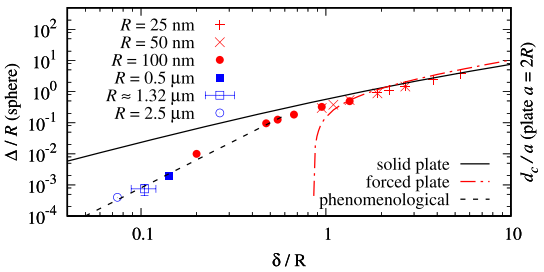

Figure 4. Scaled zero-frequency-shift separation for particles, $\Delta/R = (z_c - R)/R$ (points and dashed line, left axis), and plates (solid and dot-dashed lines, right axis) *vs* scaled penetration depth. The points correspond to simulations (red) and experiments (blue) for particles of different sizes ($R = 0.5$ μm and $R = 2.5$ μm from Olsson *et al.*,[27] and $R = 1.32$ μm from Pomorska *et al.*[9,29]). The solid line represents the plate model from eq 20, while the red dot-dashed line plots the forced plate model with displacements given by eq 28. The dashed line extrapolates simulation data (see eq 29).

particles and the QCM surface as a function of the scaled penetration depth. Rescaling the particle radius R and the penetration depth δ by the same factor results in an equivalent flow. Therefore, when we represent the zeros, z_c, of $\mathrm{Im}(Z_L) = 0$ divided by R versus δ/R for simulations of different spheres and penetration depths, they all collapse onto the same curve. The penetration depth contains the frequency dependence of z_c with respect to ω because $\delta \propto \omega^{-1/2}$. The solid line follows the plate model prediction of eq 22 for $a = 2R$, while the dashed line corresponds to the prediction of the forced plate model in this section (eqs 18 and 28, setting $\mathrm{Im}(Z_L) = 0$). The latter model gives an indication of how the acoustic response changes with the sphere dynamics, which arise from the forces induced by the surrounding flow. For large values of δ/R (low frequencies or small particles), we observe similar crossover values for the plates and particles. Clearly, the theories for plates depart from the behavior of spheres when the penetration depth becomes comparable to the sphere radius, with significant deviations when $\delta/R < 1.25$. For a QCM frequency of 35 MHz, this corresponds to spheres with $R > 50$ nm. Close to this penetration depth $\delta/R \approx 1.25$, the forced plate model yields slightly better predictions, suggesting that the crossover height decreases more quickly than in the solid plate model because of the sphere dynamics. However, as δ/R is further decreased, the forced plate model largely overestimates the decay of the cross-over distance. When the spheres lie close to the resonator ($\delta/R < 1.25$), multiple hydrodynamic reflections between the resonator and the particle determine the flow and hydrodynamic impedance.

Encouraged by the good agreement with the simple one-dimensional theory in the case of small particles, we decided to extrapolate the results obtained from three-dimensional simulations to larger particles. In particular, we extended our simulation results for $\delta/R < 0.6$ in Figure 4 to smaller values of δ/R so as to reach micron-sized particles. The smallest value $\delta/R \approx 0.2$ of our series of simulations corresponds to a gap of $\Delta = z - R \approx 1$ nm. To extrapolate to $\delta/R < 0.2$, we fix the gap value to $\Delta = 1$ nm, which corresponds to a "molecular-contact limit". This extrapolation gives

$$\frac{\Delta}{R} \approx \gamma \left(\frac{\delta(f_c)}{R} \right)^{\beta} \tag{29}$$

where $\delta(f_c) = \sqrt{\eta/(\pi \rho f_c)}$, and we find $\gamma \approx 0.8$ and $\beta \approx 3.0$. Note that the fitting group Δ/γ somehow gathers the effect of complex three-dimensional hydrodynamics around a spherical object with a small portion of its surface connected to the wall. This leads to the following phenomenological relation for the crossing frequency

$$f_c = \frac{\gamma^{2/\beta} \eta}{\pi \rho \Delta^{2/\beta}} R^{2/\beta - 2} \tag{30}$$

which suggests that $f_c \sim R^{-4/3}$.

We will now compare this trend with available experimental results, beginning with the experiments by Pomorska *et al.*,[9,29] which provide evidence in favor of the validity of our extrapolation. In the experiments, the particles and surface were decorated with polyelectrolytes of opposite charge to ensure a strong attractive potential and adhesion. A case for which $\Delta f = 0$ at approximately 15 MHz was reported corresponding to the formation of roughly spherical adsorbed clusters of nanoparticles.[9] Analyzing the field emission scanning electron microscopy images presented in their Figure 4c[29] (a close-up image is shown in Figure 2 in their 2010 paper[9]), we estimate an average radius of $R = (1.32 \pm 0.08)$ μm for the nanoclusters. Inserting the experimental data in eq 29 outputs the blue square in Figure 4, which falls nicely onto the extrapolated trend.

A second set of experiments by Olsson *et al.*[27] considered streptavidin-decorated silica particles adsorbed onto a biotinylated silica surface. In that case, the strong streptavidin-biotin links gradually adsorbed the particles, and the results for the crossover frequency vary only mildly with the ionic strength, which decreases from 8.5 MHz at 1 mM to about 7.5 MHz beyond 50 mM. Figure 4 shows that this estimation also lies on the extrapolated trend 30. We would like to take a step further in the analysis of these set of experiments to illustrate to what extent molecular forces can modify the acoustic signals. In particular, Olsson *et al.*[27] suggests that the "contact size" of individual particles probably softens with increasing ion concentration. If the biotin linker relaxes, this might lead to a small increase in the average height of the particles over the resonator, and this would hydrodynamically induce a decrease in f_c. Thus, both the contact model used by Olson[27] and the hydrodynamic trend we find here point in the same direction. An interesting, though by no means rigorous, estimation of the separation Δ follows from eq 29 for these experiments. We see that Δ increases by about 0.5 nm as the ionic strength goes from 1 to 50 mM, consistent with variations at the molecular length scales. The results suggest that the sensitivity of the QCM could also be applied to the determination of distances, in addition to

https://dx.doi.org/10.1021/acs.langmuir.0c01429
Langmuir XXXX, XXX, XXX−XXX

masses. A rigorous approach to contact forces lies beyond the scope of the present contribution, but this example illustrates the importance of considering both hydrodynamics and contact forces for theoretical analyses of the QCM to become quantitative.

Following this line of reasoning, we consider another set of experiments by Olsson *et al.*[27] where the authors observed silica particles over a bare silica surface in a (1:1) electrolyte (K^+, Cl^+) at different ionic strengths (from 0 to 150 mM). Metallurgical microscopy determined that the particles performed Brownian motion above the surface. Adding enough electrolyte (at concentration c_e = 150 mM) reduced the Brownian motion, indicating the screening of repulsive electrostatic forces and adsorption by dispersion (van der Waals) forces. Although not explicitly mentioned in the paper,[27] at smaller ionic strengths, one expects to find the silica particles suspended over the resonator and exposed to the wall-interaction potential. According to the DLVO theory, at low ionic strengths, below the critical coagulation concentration, c_{ccc}, this potential has a secondary minimum at a distance of about $\Delta \approx 6/\kappa$ (κ stands for the Debye−Hückel screening length.[33] For $c_e > c_{ccc}$, the particles start to adhere to the surface because of dispersion forces. For a KCl electrolyte in water, the Debye length ($\kappa^{-1} \propto c_e^{-1/2}$) is about 10 nm for $c_e \approx 1$ mM. Taking the values of the crossover frequency f_c reported by Olsson *et al.* (which grow with the ionic strength), we can again use eq 29 to estimate the gap Δ between the silica particles and the surface. Notably, the result of this crude estimation agrees with distances Δ decreasing with c_e as $d \sim 6/\kappa$, which points to an acoustic response governed by hydrodynamics in these experiments. A quantitative prediction would require an elaborate theory, which should weight the impedance-height dependence and the hydrodynamic propagation of long-range forces and include a more complete set of experimental details (*e.g.*, surface charge values). In this vein, we have recently carried out a detailed analysis in the case of suspended liposomes tethered to DNA strands.[15] The close agreement between experiments and simulations confirmed the dominant role of the hydrodynamic impedance when dealing with suspended particles and enabled quantitative predictions.

In summary, our analyses provide evidence that the leading contribution to the load impedance created by analytes immersed in liquids comes from hydrodynamics. While we have recently proved this claim in the case of suspended particles (liposomes tethered to DNA[15]), in the case of adsorbed particles, our findings indicate the need for first-principle hydrodynamics to enable quantitative estimations of adhesion forces from QCM analyses. This statement also applies to other types of forces, such as elastic or viscous forces, arising from the immersed structures. The following sections present a simplified analysis of some of these scenarios.

Elastic Layer. Let us replace the solid plate with an elastic layer of thickness a, density ρ' and shear modulus μ (Figure 5a). Within the layer, we denote the displacement of a point at height z and time t along the x direction with $\tilde{\phi}(z, t)$, which must satisfy the equation of motion[25]

$$\frac{\partial^2 \tilde{\phi}(z,\ t)}{\partial t^2} = \frac{\mu}{\rho'} \frac{\partial^2 \tilde{\phi}(z,\ t)}{\partial z^2} \tag{31}$$

a wave equation with speed $c = \sqrt{\mu/\rho'}$. The steady-state solution at frequency ω equals

$$\tilde{\phi}(z,\ t) = \mathrm{Re}((Ce^{-ikz} + De^{ikz})e^{-i\omega t}) \tag{32}$$

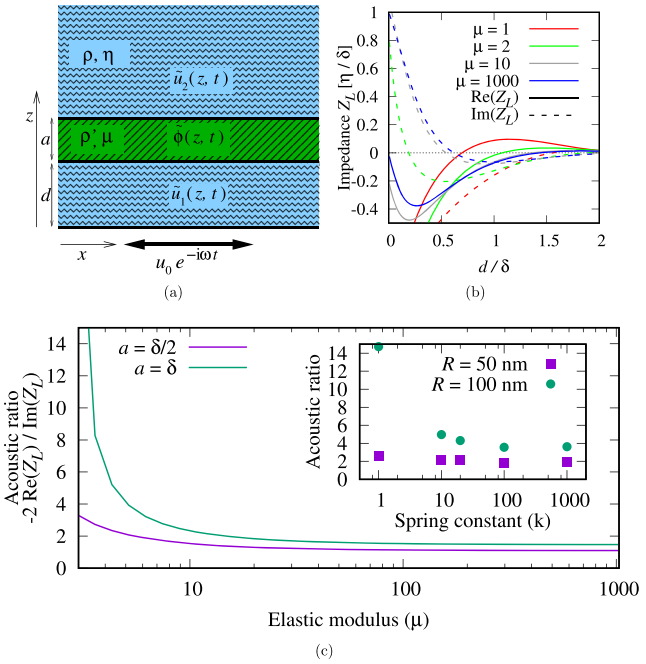

Figure 5. (a) Simple model of an elastic layer, where an elastic material of density ρ' and shear modulus μ replaces the plate. The function $\tilde{\phi}(z, t)$ indicates the displacement in the x direction at height z and time t within the layer. (b) Impedance due to an elastic layer of density $\rho' = \rho$ and thickness $a = \delta/\sqrt{2}$ as a function of the distance d to the lower plane. As the material becomes more rigid, the curves approach the solution for the solid plate (compare the curve for μ = 1000 to the green line for $\rho' = \rho$ in Figure 1b). (c) Acoustic ratio of a neutrally buoyant elastic layer of thickness a *vs* shear modulus μ at $d = 0.18\delta$, compared to simulations of spherical liposomes of radius R at height $d + R$ as a function of the elastic strength of the bonds used to connect neighboring elements in the numerical model (inset).

with $k = \omega/c$. Imposing the boundary conditions on $\tilde{u}_1$, $\tilde{u}_2$, and $\tilde{\phi}$, which amount to continuity in the speeds and stresses plus the no-slip condition at $z = 0$ and vanishing velocity as z tends toward infinity

$$\tilde{u}_1(0,\ t) = u_0 e^{-i\omega t} \tag{33}$$

$$\tilde{u}_1(d,\ t) = \left.\frac{\partial \tilde{\phi}}{\partial t}\right|_{z=d} \tag{34}$$

$$\tilde{u}_2(d + a,\ t) = \left.\frac{\partial \tilde{\phi}}{\partial t}\right|_{z=d+a} \tag{35}$$

$$\lim_{z\to\infty} \tilde{u}_2(z,\ t) = 0 \tag{36}$$

$$\eta \left.\frac{\partial \tilde{u}_1}{\partial z}\right|_{z=d} = \mu \left.\frac{\partial \tilde{\phi}}{\partial z}\right|_{z=d} \tag{37}$$

$$\eta \left.\frac{\partial \tilde{u}_2}{\partial z}\right|_{z=d+a} = \mu \left.\frac{\partial \tilde{\phi}}{\partial z}\right|_{z=d+a} \tag{38}$$

we obtain, with the help of some computer algebra, the following value for the load impedance

https://dx.doi.org/10.1021/acs.langmuir.0c01429
Langmuir XXXX, XXX, XXX−XXX

$$Z_L = \frac{2\alpha\eta(1-\Lambda^2)(e^{2ia\omega/c}-1)}{e^{2\alpha d}((1+\Lambda)^2 - e^{2ia\omega/c}(1-\Lambda)^2) + (1-\Lambda^2)(e^{2ia\omega/c}-1)} \tag{39}$$

Λ represents the dimensionless parameter

$$\Lambda = \frac{\alpha\eta}{\rho' c} = \frac{\alpha\eta}{\sqrt{\rho'\mu}} \tag{40}$$

proportional to the ratio of the velocity of viscous diffusion over δ to the speed of elastic waves, c. The other relevant groups are phase lags, $a\omega/c$, and αd.

When the elastic medium becomes rigid ($c \to \infty$, $\Lambda \to 0$), we recover the solution for the rigid plate. Figure 5b plots the impedance due to the layer as a function of the distance d that separates it from the vibrating plane.

Using the computational methods mentioned in the previous section, we simulated elastic neutrally buoyant liposomes using an elastic network made up of elements connected by harmonic bonds of the spring constant k. We observed that the acoustic ratio decreased as we increased k. Increasing the rigidity of our layer leads to similar predictions (see Figure 5c).

Fluid Layer. Lastly, we will work out the impedance for a plane fluid layer of density ρ', shear viscosity η', and velocity field $u'(z, t)$. Figure 6a displays a sketch of the system. Once

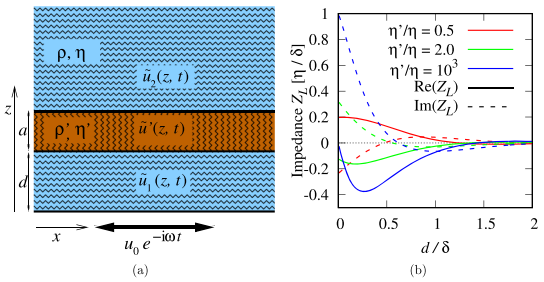

Figure 6. (a) Simple model of a fluid layer, with a liquid of density ρ' and shear viscosity η' instead of a solid layer. The function $u'(z, t)$ names the velocity field inside the layer. (b) Impedance due to a fluid layer of density $\rho' = \rho$ and thickness $a = \delta/\sqrt{2}$ as a function of the distance d to the lower plane. As the viscosity increases, the curves look more and more like those of the solid plate (the curves for $\eta'/\eta = 10^3$ resemble the green lines for $\rho' = \rho$ in Figure 1b).

again, we express the fluid velocities with eq 6 and impose the appropriate boundary conditions (continuity of velocities and stress, no slip at the lower boundary, and vanishing velocity as z tends toward infinity). The resulting load impedance equals

$$Z_L = \frac{2\alpha\eta e^{-2\alpha d}\tanh(\alpha' a)(1-\Upsilon^2)}{\tanh(\alpha' a)(1+e^{-2\alpha d}+\Upsilon^2(1-e^{-2\alpha d})) + 2\Upsilon} \tag{41}$$

with

$$\alpha' = (1-i)\sqrt{\frac{\omega\rho'}{2\eta'}} \tag{42}$$

and

$$\Upsilon = \frac{\alpha'\eta'}{\alpha\eta} \tag{43}$$

Figure 6b shows the change in the impedance of the fluid layer as a function of the distance d to the lower plane for different values of the shear viscosity. As the viscosity increases, the curves approach the solid plate limit. Interestingly, a layer viscosity lower than that of the surrounding fluid leads to a flip in the behavior of the real and imaginary parts of Z_L, as observed in QCM experiments with nanobubbles[30−32] (in the figure, compare the red line for $\eta'/\eta = 0.5$ to the green line for $\eta'/\eta = 2$).

CONCLUSIONS

In addition to providing analytical expressions for the load impedance of different types of immersed layers, we have demonstrated the importance of considering the role of hydrodynamics in explaining the effects of these layers on the QCM. Although we have not considered any contact forces between the load and the QCM, the models explained above predict the behavior of suspended loads and recover the expected Sauerbrey relation in the limit of adsorbed layers. Furthermore, the "vanishing mass" phenomenon observed in suspensions arises as a natural consequence in our derivations.

The analytical treatment contained in this work assumes stick boundary conditions at the liquid−QCM interface (a rather safe approximation for charged surfaces[34] or sensors decorated with proteins or other molecules acting as linkers).[15] However, experimental research has shown considerable slippage lengths for low-viscosity liquids, especially for a hydrophobic-coated QCM.[35] Note that a slip length of $b \sim 10$ nm would typically be considered a slippery surface, and if we were to take this effect into account, it would decrease the interfacial stress modifying our expressions with a contribution proportional to b/δ.[36] The analytical derivation would involve changing the boundary condition on the QCM surface from $u(0) = u_0$ to $u(0) - u_0 = b\frac{\partial u}{\partial z}$.

The evidence provided here strongly suggests that other types of suspensions (such as the simulated suspended spheres considered above) share the same generic features. Even though the plates in Figure 3 had an impedance about five times greater than the spheres, the dependence on height displayed surprisingly parallel behaviors. Prefactors cancel out when calculating the acoustic ratio; so, the plate acoustic ratios provide a decent estimate of the value measured for the sphere (see Figure 7).

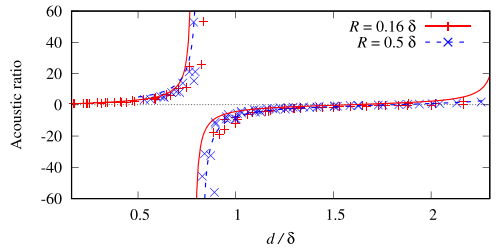

Figure 7. Acoustic ratio *vs* height over the QCM for neutrally buoyant spheres (points) and the solid plate (lines). The distance d indicates the separation between the plate and QCM and the distance from the center of the sphere to the QCM.

The preceding pages show that large acoustic ratios do not necessarily imply large values of the dissipation. As we have seen, vanishing frequency shifts naturally lead to diverging acoustic ratios.

Finally, we considered the crossover to positive frequency shifts and compared the analytical prediction of the one-dimensional plate system to simulations of submicron spheres

https://dx.doi.org/10.1021/acs.langmuir.0c01429
Langmuir XXXX, XXX, XXX−XXX

and experiments carried out with micron-sized colloids. The plate model correctly predicts the zero-frequency crossover for small enough particles. We observe a transition to a large particle regime when the dimensionless parameter R/δ becomes large enough ($R/\delta > 0.8$). The one-dimensional theories clearly fail in this regime. By contrast, our three-dimensional simulations correctly extrapolate to larger (micron-sized) colloids, even with the latter adsorbed to the wall. As we did not consider adhesive forces, such an agreement highlights the role of hydrodynamics in determining the response of large adsorbed particles, and calls for a hydrodynamic extension of the existing contact-force and elastic-stiffness QCM theories. The "coupled-resonance model", which predicts positive shifts within the "elastic loading" regime in the QCM[3,7] was originally derived for spheres in the dry state but has subsequently been applied extensively in liquids.[3,9,27] Our results call for a revision of the role of contact forces and elastic stiffness in liquids, an investigation which requires a generalization of existing theories including the difficult topic of elastohydrodynamic lubrication.[37] Advancing our theoretical understanding in this direction would greatly improve the predictive power of QCM analyses of molecular and mesoscopic contact forces.

APPENDIX A

Average Velocity Integrals

The velocities $\tilde{v}_s$ and $\tilde{v}_v$ in eq 26 come from averaging the flow profile $u(z, t)$ over the surface and volume of the sphere, respectively

$$\overline{v}_s = \frac{1}{4\pi r^2}\int_S u_0 e^{-\alpha z}\, \mathrm{d}\mathbf{S} \tag{44}$$

$$\overline{v}_v = \frac{3}{4\pi r^3}\int_V u_0 e^{-\alpha z}\, \mathrm{d}\mathbf{V} \tag{45}$$

To carry out the first of these integrals, we choose spherical coordinates around the center of the immersed sphere at height d. Therefore

$$\int_S u(z,\ t)\mathrm{d}\mathbf{S} = \int_0^{2\pi}\left(\int_0^{\pi} u_0 e^{-\alpha(d+r\cos(\theta))} r^2 \sin(\theta)\mathrm{d}\theta\right)\mathrm{d}\phi \tag{46}$$

After integrating over ϕ

$$\begin{aligned}\int_S u(z,\ t)\mathrm{d}\mathbf{S} &= 2\pi u_0 r e^{-\alpha d}\int_0^{\pi} e^{-\alpha r\cos(\theta)} r\sin(\theta)\mathrm{d}\theta \\ &= 2\pi u_0 r e^{-\alpha d}\left[\frac{e^{-\alpha r\cos(\theta)}}{\alpha}\right]_0^{\pi}\end{aligned} \tag{47}$$

Hence

$$\overline{v}_s = \frac{u_0 e^{-\alpha d}}{\alpha r}\sinh(\alpha r) \tag{48}$$

The volume integral is simply equal to the integral over the radius of the surface integral from 0 to the radius of the sphere r

$$\begin{aligned}\int_V u(z,\ t)\mathrm{d}\mathbf{V} &= \int_0^{r}\frac{4\pi r' u_0}{\alpha} e^{-\alpha d}\sinh(\alpha r')\mathrm{d}r' \\ &= \frac{4\pi u_0}{\alpha} e^{-\alpha d}\left[\frac{r'\cosh(\alpha r')}{\alpha} - \frac{\sinh(\alpha r')}{\alpha^2}\right]_0^{r}\end{aligned} \tag{49}$$

from which we get

$$\overline{v}_v = \frac{3u_0}{\alpha r^3} e^{-\alpha d}\left(\frac{r\cosh(\alpha r)}{\alpha} - \frac{\sinh(\alpha r)}{\alpha^2}\right) \tag{50}$$

AUTHOR INFORMATION

Corresponding Authors

Marc Meléndez − *Department of Theoretical Condensed Matter Physics, Universidad Autónoma de Madrid, 28049 Madrid, Spain;* orcid.org/0000-0001-5198-3586; Email: marc.melendez@uam.es

Rafael Delgado-Buscalioni − *Department of Theoretical Condensed Matter Physics, Universidad Autónoma de Madrid, 28049 Madrid, Spain; Institute for Condensed Matter Physics, IFIMAC, 28049 Madrid, Spain;* orcid.org/0000-0001-6637-2091; Email: rafael.delgado@uam.es

Author

Adolfo Vázquez-Quesada − *Departamento de Física y Matematicas, Universidad de Alcalá, 28871 Madrid, Spain*

Complete contact information is available at: https://pubs.acs.org/10.1021/acs.langmuir.0c01429

Notes

The authors declare no competing financial interest.

ACKNOWLEDGMENTS

Our research here was supported by the European Commission FETOPEN Horizon 2020 Catch-U-DNA project. R.D.-B. also acknowledges funding from the Spanish MINECO project FIS2017-86007-C3-1-p.

ADDITIONAL NOTE

[a]We note that recent (yet unpublished) experiments performed with 20 nm-diameter liposomes at 150 MHz by the Gizelli group within the CATCH-U-DNA project present such a transient increase with $\Delta f > 0$ at short times after the injection of liposomes.

REFERENCES

(1) Sauerbrey, G. Verwendung von Schwingquarzen zur Wägung dünner Schichten und zur Mikrowägung. *Z. Phys.* **1959**, *155*, 206−222.

(2) Nomura, T.; Okuhara, M. Frequency shifts of piezoelectric quartz crystals immersed in organic liquids. *Anal. Chim. Acta* **1982**, *142*, 281−284.

(3) Johannsmann, D. *The Quartz Crystal Microbalance in Soft Matter Research. Fundamentals and Modeling*; Springer, 2015.

(4) Johannsmann, D. Viscoelastic, mechanical and dielectric measurements on complex samples with the quartz crystal microbalance. *Phys. Chem. Chem. Phys.* **2008**, *10*, 4516−4534.

(5) Lane, T. J. *Ultrasonic Rheology of Mixed-Phase Systems: Using a QCM as an Effective Rheological Device-Theory, Amphiphiles: Molecular Assembly and Applications*; American Chemical Society, 2011; pp 145−174.

(6) Voinova, M. V.; Jonson, M.; Kasemo, B. Missing mass effect in biosensor's QCM applications. *Biosens. Bioelectron.* **2002**, *17*, 835−841.

(7) Dybwad, G. L. A sensitive new method for the determination of adhesive bonding between a particle and a substrate. *J. Appl. Phys.* **1985**, *58*, 2789−2790.

(8) Marxer, C. G.; Coen, M. C.; Greber, T.; Greber, U. F.; Schlapbach, L. Cell spreading on quartz crystal microbalance elicits positive frequency shifts indicative of viscosity changes. *Anal. Bioanal. Chem.* **2003**, *377*, 578−586.

(9) Pomorska, A.; Shchukin, D.; Hammond, R.; Cooper, M. A.; Grundmeier, G.; Johannsmann, D. Positive frequency shifts observed

https://dx.doi.org/10.1021/acs.langmuir.0c01429
Langmuir XXXX, XXX, XXX−XXX

upon adsorbing micron-sized solid objects to a quartz crystal microbalance from the liquid phase. *Anal. Chem.* **2010**, *82*, 2237−2242.
(10) Kravchenko, S.; Snopok, B. "Vanishing mass" in the Sauerbrey world: quartz crystal microbalance study of self-assembled monolayers based on a tripod-branched structure with tuneable molecular flexibility. *Analyst* **2020**, *145*, 656−666.
(11) Tellechea, E.; Johannsmann, D.; Steinmetz, N. F.; Richter, R. P.; Reviakine, I. Model-Independent Analysis of QCM Data on Colloidal Particle Adsorption. *Langmuir* **2009**, *25*, 5177−5184.
(12) Lapidot, T.; Sedransk Campbell, K. L.; Heng, J. Y. Y. Model for Interpreting Surface Crystallization Using Quartz Crystal Microbalance: Theory and Experiments. *Anal. Chem.* **2016**, *88*, 4886−4893.
(13) Gillissen, J. J. J.; Jackman, J. A.; Tabaei, S. R.; Cho, N.-J. A Numerical Study on the Effect of Particle Surface Coverage on the Quartz Crystal Microbalance Response. *Anal. Chem.* **2018**, *90*, 2238−2245.
(14) Gillissen, J. J. J.; Jackman, J. A.; Tabaei, S. R.; Yoon, B. K.; Cho, N.-J. Quartz Crystal Microbalance Model for Quantitatively Probing the Deformation of Adsorbed Particles at Low Surface Coverage. *Anal. Chem.* **2017**, *89*, 11711−11718.
(15) Vázquez-Quesada, A.; Meléndez, M.; Tsortos, A.; Mateos-Gil, P.; Miloni, D.; Gizeli, E.; Delgado-Buscalioni, R. Hydrodynamics of Quartz-Crystal-Microbalance DNA Sensors Based on Liposome Amplifiers. *Phys. Rev. Appl.* **2020**, *13*, 064059.
(16) Gillissen, J. J. J.; Tabaei, S. R.; Jackman, J. A.; Cho, N.-J. A model derived from hydrodynamic simulations for extracting the size of spherical particles from the quartz crystal microbalance. *Analyst* **2017**, *142*, 3370−3379.
(17) Milioni, D.; Mateos-Gil, P.; Papadakis, G.; Tsortos, A.; Sarlidou, O.; Gizeli, E. Acoustic Methodology for Selecting Highly Dissipative Probes for Ultrasensitive DNA Detection. *Anal. Chem.* **2020**, *92*, 8186−8193.
(18) Johannsmann, D.; Reviakine, I.; Rojas, E.; Gallego, M. Effect of sample heterogeneity on the interpretation of QCM (-D) data: comparison of combined quartz crystal microbalance/atomic force microscopy measurements with finite element method modeling. *Anal. Chem.* **2008**, *80*, 8891−8899.
(19) Johannsmann, D.; Reviakine, I.; Richter, R. P. Dissipation in films of adsorbed nanospheres studied by quartz crystal microbalance (qcm). *Anal. Chem.* **2009**, *81*, 8167−8176.
(20) Reviakine, I.; Johannsmann, D.; Richter, R. P. Hearing what you cannot see and visualizing what you hear: interpreting quartz crystal microbalance data from solvated interfaces. *Anal. Chem.* **2011**, *83*, 8838−8848.
(21) Tsortos, A.; Papadakis, G.; Mitsakakis, K.; Melzak, K. A.; Gizeli, E. Quantitative determination of size and shape of surface-bound DNA using an acoustic wave sensor. *Biophys. J.* **2008**, *94*, 2706−2715.
(22) Balboa, F.; Bell, J. B.; Delgado-Buscalioni, R.; Donev, A.; Fai, T. G.; Griffith, B. E.; Peskin, C. S. Staggered Schemes for Fluctuating Hydrodynamics. *Multiscale Model. Simul.* **2012**, *10*, 1369.
(23) Peskin, C. S. The immersed boundary method. *Acta Numer.* **2002**, *11*, 479−517.
(24) Stokes, G. G. On the effect of the internal friction of fluids on the motion of pendulums. *Trans. Cambridge Philos. Soc.* **1851**, *9*, 8.
(25) Kanazawa, K. K.; Gordon, J., II The oscillation frequency of a quartz resonator in contact with a liquid. *Anal. Chim. Acta* **1985**, *175*, 99−105.
(26) Landau, L. D.; Lifshitz, E. M. *Fluid Mechanics*; Pergamon Press, 1987; pp 83−92.
(27) Olsson, A. L. J.; van der Mei, H. C.; Johannsmann, D.; Busscher, H. J.; Sharma, P. K. Probing Colloid-Substrate Contact Stiffness by Acoustic Sensing in Liquid Phase. *Anal. Chem.* **2012**, *84*, 4504−4512.
(28) Mazur, P.; Bedeaux, D. A generalization of Faxén's theorem to nonsteady motion of a sphere through an incompressible fluid in arbitrary flow. *Physica* **1974**, *76*, 235−246.
(29) Pomorska, A.; Yliniemi, K.; Wilson, B. P.; Shchukin, D.; Johannsmann, D.; Grundmeier, G. QCM study of the adsorption of polyelectrolyte covered mesoporous TiO_2 nanocontainers on SAM modified Au surfaces. *J. Colloid Interface Sci.* **2011**, *362*, 180−187.
(30) Du, B.; Goubaidoulline, I.; Johannsmann, D. Effects of Laterally Heterogeneous Slip on the Resonance Properties of Quartz Crystals Immersed in Liquids. *Langmuir* **2004**, *20*, 10617−10624.
(31) Zhang, X. H. Quartz crystal microbalance study of the interfacial nanobubbles. *Phys. Chem. Chem. Phys.* **2008**, *10*, 6842−6848.
(32) Ondarçuhu, T. *Nanoscale Liquid Interfaces: Wetting, Patterning and Force Microscopy at the Molecular Scale*; Taylor & Francis, 2013.
(33) Israelachvili, J. N. *Intermolecular and Surface Forces*, 3rd ed.; Academic Press, 2010.
(34) Xie, Y.; Fu, L.; Niehaus, T.; Joly, L. Liquid-Solid Slip on Charged Walls: The Dramatic Impact of Charge Distribution. *Phys. Rev. Lett.* **2020**, *125*, 014501.
(35) Ferrante, F.; Kipling, A. L.; Thompson, M. Molecular slip at the solid-liquid interface of an acousticwave sensor. *J. Appl. Phys.* **1994**, *76*, 3448.
(36) Qiao, X.; Zhang, X.; Tian, Y.; Meng, Y. Modeling the response of a quartz crystal microbalance under nanoscale confinement and slip boundary conditions. *Phys. Chem. Chem. Phys.* **2015**, *17*, 7224−7231.
(37) Gohar, R. *Elastohydrodynamics*; World Scientific, 2001.
(38) Balboa-Usabiaga, F. FLUAM. https://github.com/fbusabiaga/fluam/ (accessed September 10, 2019).

https://dx.doi.org/10.1021/acs.langmuir.0c01429
Langmuir XXXX, XXX, XXX−XXX